

Electron-phonon coupling in a two-dimensional inhomogeneous electron gas: consequences for surface spectral properties

Natalia Pavlenko^{1,2} and Thilo Kopp¹

¹ Center for Electronic Correlations and Magnetism, Universität Augsburg, 86135 Augsburg, Germany

² Institute for Condensed Matter Physics, 79011 Lviv, Ukraine

PACS numbers: 74.81.-g, 74.78.-w, 73.20.Mf

Abstract. We investigate the coupling of an inhomogeneous electron system to phonons. The properties of an electronic system composed of a mixture of microscopic ordered and disordered islands are changed fundamentally by a phonon mode. In high- T_c cuprates, such a phase separation scenario is supported by recent STM and nuclear quadrupole resonance studies. We show that even a weak or moderate electron-phonon coupling can be sufficient to produce dramatic changes in the electronic state of the inhomogeneous electron gas. The spectral properties calculated in our approach provide a natural explanation of the low-energy nodal ARPES features and exhibit a novel non-Fermi-liquid state stabilized through electron-phonon coupling.

Submitted to: *J. Phys.: Condens. Matter*

1. Introduction

An eminent feature observed in the angle-resolved photoemission spectroscopy (ARPES) studies of high- T_c cuprates is the kink-like change of electron velocity, interpreted in terms of the coupling to oxygen phonon modes [1, 2]. These kinks are associated with a distinct break-up of the spectral weight into a high-intensity part which develops near the Fermi surface, and a broad structure of less intensity at higher energies below the Fermi level. Despite the structural differences between various types of cuprates, the peculiarities in the dispersion at 50–80 meV were detected in $\text{Bi}_2\text{Sr}_2\text{CaCu}_2\text{O}_{8+\delta}$ (Bi2212), $\text{La}_{2-x}\text{Sr}_x\text{CuO}_4$ (LSCO), $\text{YBa}_2\text{Cu}_3\text{O}_{6+x}$ (YBCO) and other related systems [1, 2, 3, 5, 4, 6], and are believed to shed light on the microscopic mechanism of high- T_c superconductivity. Although significant efforts have been directed towards a theoretical investigation of the influence of many-body interactions on the one-electron properties of Hubbard and t - J models, typically used for cuprates [7], the origin of the nodal ARPES features and of their unusual doping and temperature behavior still remains an open question.

Many-body effects are known to produce changes in the electronic dispersion, as deduced from electronic photoemission spectra. One mechanism, which was shown to cause low-energy kinks, is controlled by a strong electron-phonon coupling in the free electron gas [8, 9]. This coupling leads to a renormalization of the electron effective mass in the energy range close to the Fermi energy E_F , below a characteristic phonon frequency ω_{ph} : $E - E_F < \omega_{\text{ph}}$. On the other hand, when the electrons in a metal are strongly correlated, a purely electronic mechanism can also lead to dispersion kinks which have been related to a crossover between Fermi- and non-Fermi-liquid behavior [10].

In the analysis of ARPES intensities, one should always consider the fact that photoemission experiments analyze electronic surface and subsurface states which brings the near-surface correlations into the focus. Due to the strong interaction of these electrons with subsurface phonon modes and virtual charge transfer excitations, the effect of such collective modes on the electronic subsystem is crucial [11, 12]. A direct consequence of these interactions is a significant reduction of the local Hubbard repulsion to values well below the electronic bandwidth $8t$, where t is the electron hopping. This finding allows to suggest that mechanisms different from the purely electronic could play a role in the appearance of the dispersion kinks in cuprates. As the coupling with magnons cannot satisfactorily explain the doping and temperature behavior of such kinks, we will focus on the analysis of the interaction with phonons.

In the high- T_c cuprates another important factor, which has to be addressed in studies of their electronic properties, is charge inhomogeneity. In the pseudogap state and in regimes with suppressed superconductivity, scanning tunneling microscopy (STM) experiments indicate a local electron order [13, 14, 15, 16, 21, 22, 23, 24]. This, together with nuclear quadrupole resonance (NQR) and resonant soft X-ray scattering studies [25, 26, 27, 28], provides strong support for a state of electronic

phase separation as one of the widely discussed scenarios for under- and optimal-doped cuprates [13, 15, 16, 25, 26, 27]. Such a state exhibits a mixture of microscopic charge ordered (characterized as “more insulating” with suppressed local density of states) and charge disordered uniform (metallic) domains with a dominance of the metallic phase at higher doping levels [16]. The ARPES intensities obtained for the electronic phase separated state inevitably contain the contributions from both types of domains. This fact can be easily understood since the electrons collected on the ARPES analyzer can be emitted from the disordered as well as from the ordered surface islands. Due to the quantum nature of the collected electrons, they cannot be described in terms of pure “ordered” or “disordered” electron wave functions, but rather as a superposition of both states. Therefore, in order to understand ARPES intensities within such an inhomogeneous scenario, we need to analyze the consequences of the electron-phonon coupling not only for the disordered, but also for the ordered sections of the surface.

In the hole-doped cuprates, the recent ab-initio studies have demonstrated a weakness of the electron-phonon coupling which should result in a negligibly small contribution to the formation of the dispersion kinks [17, 18]. Despite the different approaches, these works have been focused on the electronic homogeneous state, without any serious attention to a possible electronic charge order. As a consequence of such a predominant consideration of the uniform electronic state, the general view about a relative unimportance of the electron-phonon coupling for the electronic properties of the copper oxide planes became widely accepted in the literature. In an altering approach, the strongly inhomogeneous interactions of the electrons to several optical phonon modes (buckling and breathing) has been proposed [19] which was not really successful in the explanation of real physical mechanisms of spectral anomalies in the cuprates.

In the present work, we analyze the electron-phonon coupling in the charge-ordered state. We show that in contrast to the uniform electron gas, in the ordered system even a weak or moderate coupling to an optical phonon mode produces dramatic changes in the electronic properties and leads to a formation of new electronic state which cannot be described by a standard Fermi-liquid theory. Due to significant advances achieved in the recent STM studies of the cuprates [13, 20], the existence of local electron order in these systems becomes rather a well established fact. To make a step towards an interpretation of the spectral features in the context of the inhomogeneous state observed in the STM studies, the inhomogeneous surface in our work is described as a mixture of the electronically uniform and ordered states. We obtain that the superposition of these states produces several distinct features and a characteristic intensity break-up in the electronic spectral maps. In our work, we connect this break-up with the spectral anomalies observed in the cuprates. Consequently, the proposed approach is expected to shed new light on the mechanisms of kinks and on the origin of non Fermi-liquid behavior detected in these systems.

2. Electronic spectral properties in the charge-ordered state

To gain deeper insight into the ordered surface state, we provide a comparison of a disordered two-dimensional electron gas, characterized by a free tight-binding dispersion $\varepsilon_0(\mathbf{k})$, with an ordered electron system, both coupled to an optical phonon mode with a frequency $\omega_{\text{ph}} = \omega_0$. In our studies, we take into account the Coulomb interaction V between nearest neighbors

$$H_{\text{el}} = \sum_{\mathbf{k},\sigma} \varepsilon_0(\mathbf{k}) n_{\mathbf{k}\sigma} + V \sum_{\langle ij \rangle} n_i n_j \quad (1)$$

where $n_{\mathbf{k}\sigma}$ are the electron number operators and $n_i = \sum_{\sigma} n_{i\sigma}$. The electron-phonon interaction is considered in terms of a Holstein approach

$$H_{\text{el-ph}} = -g \sum_i n_i (b_i + b_i^\dagger) + \omega_0 \sum_i b_i^\dagger b_i, \quad (2)$$

where the phonon operators refer to a vibration mode of frequency ω_0 . The parameter $g = \sqrt{\omega_0 E_p}$ (E_p is the polaron binding energy) refers the coupling of the holes in the copper oxide planes to the motion of apical oxygens in the top surface planes of the samples. In our calculations, the low-energy phonon frequency $\omega_0 = 0.05 - 0.1t$ reflects the softening of the surface optical phonon modes suggested in Ref. [12]. For the free electronic dispersion $\varepsilon_0(\mathbf{k}) = -2t\eta_{\mathbf{k}}^+ - \xi_{\mathbf{k}}$ (where $\eta_{\mathbf{k}}^+ = \cos k_x + \cos k_y$, $\xi_{\mathbf{k}} = \mu + 4t' \cos k_x \cos k_y$ and μ is the chemical potential) we choose $t = 0.18$ eV, $t' = -0.4t$, which is in the range of typical values found from fitting ARPES data for Bi2212 and Tl2201 [29, 30].

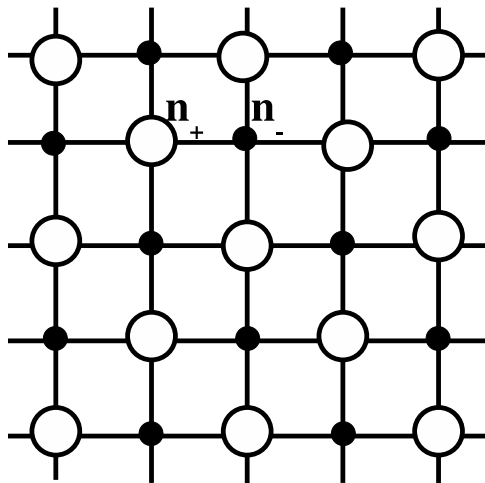


Figure 1. Schematic view of checkerboard ordering in a two-dimensional electron gas.

In our analysis we consider a checkerboard electronic ordering which introduces a doubling of the square unit cell shown in Fig. 1. This ordering is parameterized in terms of sublattice electronic occupancies n_{\pm} with order parameter $\delta = n_+ - n_-$ and average electron concentration $(n_+ + n_-)/2 = 1 - x$. The values of δ are obtained from the minimization of the mean-field type free energy. In such a charge ordered state, the electronic band structure is characterized by two subbands $\varepsilon_j(\mathbf{k}) = -\xi_{\mathbf{k}} + 4Vn \pm \Delta_{\Sigma}$.

The correction $\Delta_\Sigma = \sqrt{(2V\delta)^2 + (2t\eta_{\mathbf{k}}^+ - \Sigma_{+-}^{HF})^2}$ originates from intersublattice electron correlations, introduced through the Hartree-Fock self-energy $\Sigma_{+-}^{HF} = -\int d\mathbf{q} \sum_{\omega_n} V \cdot \eta_{\mathbf{k}-\mathbf{q}}^+ \cdot G_{+-}^{HF}(\mathbf{q}, \omega_n)$ in the Matsubara electron propagators $G_{\alpha\beta}^{HF}(\mathbf{q}, \omega_n)$. The new feature arising in the ordered band structure is the flatness of the energy subbands $\varepsilon_j(\mathbf{k})$ which is generated by their splitting through the charge-order gap $\Delta_0 = 4V\delta$, Fig. 2(a). Here, in contrast to the disordered free dispersion $\varepsilon_0(\mathbf{k})$, the emergence of the gap Δ_0 results in the formation of new local extrema of the ordered dispersions $\varepsilon_j(\mathbf{k})$. Fig. 3 shows a comparison of the detailed (k_x, k_y) map of the low-energy ordered subband $\varepsilon_2(\mathbf{k})$ with the corresponding map of the free electron dispersion $\varepsilon_0(\mathbf{k})$. One can immediately see that the electron order produces dramatic changes in the topology of the electronic structure which include (i) the formation of a new maximum in the central nodal point N = $(\pi/2, \pi/2)$ of the Brillouin zone; (ii) the appearance of new saddle points S = (k_x^S, k_y^S) . The saddle point S is located close to Γ (the second symmetric saddle point is close to Y) in the nodal direction so that $k_x^S = k_y^S = k_S$ where the coordinate k^S is given by

$$\cos k_S = \frac{\sqrt{(4t + 2VI_{+-})^4 - (16t'V\delta)^2}}{8|t'|(4t + 2VI_{+-})}, \quad (3)$$

where the quantity I_{+-} parametrizes the Hartree-Fock self-energy $\Sigma_{+-}^{HF}(\mathbf{k}) = -(V/2)\eta_{\mathbf{k}}^+ I_{+-}$. For the chosen values of the model parameters, the maximal values of I_{+-} are of the order 0.5. The expression (3) clearly shows that the saddle point S is controlled by the charge order gap and disappears for weaker Coulomb repulsion V , i. e., it is absent in the disordered uniform state with $\delta \rightarrow 0$. We also note that the nodal point N indicated in the top map of the band $\varepsilon_0(\mathbf{k})$ in Fig. 3 corresponds in fact to the intersection point of the two branches of $\varepsilon_0(\mathbf{k})$ (see Fig. 2(a)). They are generated with the convolution to the first Brillouin zone and do not show an extremum at N. In contrast to $\varepsilon_0(\mathbf{k})$, the new local extrema N and S of $\varepsilon_2(\mathbf{k})$ are well-defined and should be considered as *a generic feature of the band structure in the electron-ordered state*.

When the flat low-energy subband $\varepsilon_2(\mathbf{k})$ is coupled to the phonon mode, the local maximum at N and the saddle point at S lead to van-Hove singularities in the sublattice contributions to the electronic self-energies $\Sigma_\alpha^{ph} = -g^2 \int d\mathbf{q} \sum_{\omega_n'} G_{\alpha\alpha}^{HF}(\mathbf{k} - \mathbf{q}, \omega_n - \omega_n') D(\mathbf{q}, \omega_n')$. Here $D(\mathbf{q}, \omega_n') = 2\omega_0 / ((i\omega_n')^2 - \omega_0^2)$ is the unperturbed phonon Green function \ddagger and the one-electron sublattice propagators $G_{\alpha\alpha}^{HF}$ ($\alpha = \{+, -\}$) are calculated in the ordered electron state in the self-consistent Hartree-Fock approximation. Furthermore, the phonon scattering term can be decomposed as $\Sigma_\pm^{ph} = \Sigma_0^{ph} \mp \Delta\Sigma_0^{ph}$ where the part $\Delta\Sigma_0^{ph} \sim V\delta$ disappears in the charge disordered state. With this form of Σ_\pm^{ph} , the renormalized electronic propagators can be conveniently presented as a combination of the band Green functions $g_j = 1/(i\omega_n + \xi_{\mathbf{k}} - \Sigma_j(\mathbf{k}, \omega_n))$: $G_{\alpha\alpha} = G_0 \mp \Delta G_0$, where $G_0 = (g_1 + g_2)/2$ and $\Delta G_0 = (2V\delta + \Delta\Sigma_0^{ph})(g_1 - g_2)/(\Sigma_1 - \Sigma_2)$. In the band propagators

\ddagger As the main results for the electronic properties, including the topological anomalies of the dispersion and the NFL-state, appear already at small electron-phonon coupling $E_p/t \sim 0.2$, undressed phonon Green functions have been used in the calculations of the electronic self-energy.

g_j , the effective self-energy parts $\Sigma_j = \Sigma_0^{ph} + 4Vn \pm \sqrt{(\Delta\Sigma_0^{ph} + 2V\delta)^2 + (2t\eta_{\mathbf{k}}^+ - \Sigma_{\pm}^{HF})^2}$ contain the information about both, charge density fluctuations and electron-phonon scattering processes. We note that Σ_2 and g_2 , which determine the low-energy quasi-particle excitations, are of prime importance.

In Fig. 2(b), we show the frequency-dependent real part of $\Sigma_0^{ph}(\mathbf{k}, \omega)$ at different doping levels x . The kinks appearing in Σ_0^{ph} at $\omega = \omega_i$ ($i = 1, \dots, 3$) correspond to the van-Hove singularities in Σ_{\pm}^{ph} . In the charge disordered state, the typical van-Hove singularities in Σ_0^{ph} are caused by the local extrema in the electron dispersion $\varepsilon_0(\mathbf{k})$ which appear in the high-symmetry points Γ , Y and M of the Brillouin zone (Fig. 2(a)). In the charge ordered state, the flattening of $\varepsilon_2(\mathbf{k})$ produces the additional nodal maximum of $\varepsilon_2(\mathbf{k} = N)$ and the saddle point at $\mathbf{k} = S$ which lead to the appearance of new van-Hove singularities in Σ_{\pm}^{ph} at small ω . These low-energy singularities correspond to the peaks in $\text{Im}\Sigma_0^{ph}$ (see Fig. 4) and are related to the kinks in $\text{Re}\Sigma_0^{ph}$ (Fig. 2(b)). In the ordered state, the energies of the low-frequency singularities are determined by the equations $\omega - \varepsilon_2(\mathbf{k}_i) \pm \omega_0 = 0$ where $\mathbf{k}_i = \{\Gamma, N, S\}$. Specifically, while the maximum at $\mathbf{k} = N$ produces a jump of Σ_0^{ph} described by $\text{Im}\Sigma_0^{ph} \sim \Theta(\Omega^N - \omega)$ at small $\Omega^N = \varepsilon_2(\mathbf{k} = N) + \omega_0 > 0$, the saddle point S leads to a distinct logarithmic singular behavior of Σ_0^{ph} :

$$\begin{aligned} \text{Im}\Sigma_0^{ph} \sim & g^2[(1 + b_0 - f(\omega - \omega_0)) \log |(\Omega_2^S - \omega)/t| \\ & + (b_0 + f(\omega + \omega_0)) \log |(\Omega_3^S - \omega)/t|], \end{aligned} \quad (4)$$

where $b_0 = b(\omega_0)$ and $f(\omega)$ are the Bose and Fermi distributions functions, and the energies $\Omega_{2/3}^S = \varepsilon_2(k_S) \mp \omega_0$ are located close to the Fermi level: $\omega_3 < \Omega_2^S < \omega_2$, $\omega_2 < \Omega_3^S < 0$.

As the chemical potential directly affects ε_2 in these equations, the kinks of $\Sigma_2(\mathbf{k}, \omega)$ at $\omega = \omega_i$ which result from the new van-Hove singularities are strongly doping-dependent. It is noteworthy that these low-frequency kinks at $\omega = \omega_i$ ($i = 1, \dots, 3$) shown in Fig. 2(b) will inevitably change the one-electron spectral properties near the Fermi level. To see this, we present in Fig. 2(c) the low-energy dispersion $E_2(\mathbf{k})$ of the underdoped system ($x = 0.11$), now calculated from the equation $\omega + \xi_{\mathbf{k}} - \Sigma_2(\mathbf{k}, \omega) = 0$ for the poles of the renormalized electron propagators for different values of electron-phonon coupling. A central property resulting from the new van-Hove singularities is a topological reconstruction of $E_2(\mathbf{k})$ close to the N-point. In Fig. 2(c), (case $E_p = 0.8t$), this reconstruction corresponds to a transformation of the maximum $E_2(\mathbf{k} = N)$ into a new singular hat-shaped band region which appears above a critical value $E_p^* \approx 0.2t$.

The novel nodal dispersion exhibits a nonanalytic character in the symmetric regions n_1 and n_2 near the Fermi-level. In these regions, $E_2(\mathbf{k})$ is a multi-valued function of \mathbf{k} . The two extra subbranches of E_2 emerge from the additional poles of the one-electron Green function and are caused by the van-Hove kinks in $\Sigma_0^{ph}(\mathbf{k}, \omega)$. In the singular points S_1 and S_2 of the regions n_1 and n_2 which connect monotonically decreasing and increasing branches of $E_2(\mathbf{k})$, the nodal electron velocity $v = |\nabla_{\mathbf{k}} E_2(\mathbf{k})|$ approaches infinite values. The range \mathbf{k} close to \mathbf{k}_F with singular v is separated from

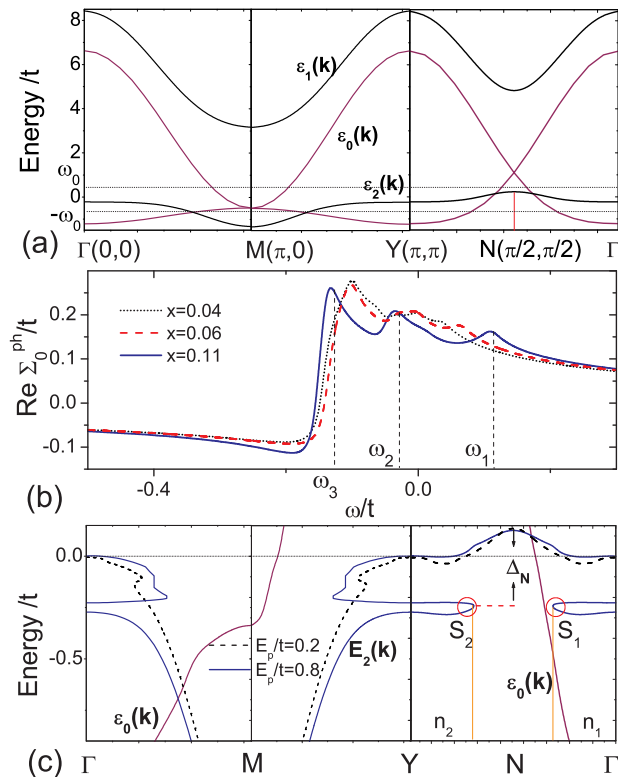


Figure 2. Electronic band structure and self energy for a charge ordered system coupled to phonons where $V/t = 1.3$. (a) Band structure with vanishing phonon coupling in the ordered and charge disordered uniform states, where the dotted lines refer to $\pm\omega_0 = 0.5t$. Here $kT/t = 0.03$ and $x = 0.11$. (b) Real part of $\Sigma_0^{ph}(\mathbf{k}, \omega)$ calculated in the ordered state with $\omega_0 = 0.05t$ for different doping levels. Here \mathbf{k} is located in the nodal region close to the point $N = (\pi/2, \pi/2)$ of the Brillouin zone; $|\mathbf{k}| = 0.9$, $kT/t = 0.03$ and $E_p = 1.2t$. (c) Evolution of the renormalized low-energy band structure in the ordered state with increasing E_p for $x = 0.11$ and $\omega_0 = 0.05t$. The transition at $E_p = E_p^* \approx 0.2t$ is characterized by a transformation of the local maximum $E_2(\mathbf{k} = N)$ into a hat-shaped structure and by the buildup of a singular $E_2(\mathbf{k})$ in the regions n_1 and n_2 with singular electron velocity v . The regions $\mathbf{k} \sim \mathbf{k}_F$ are separated by a gap Δ_N from $\mathbf{k} \sim N$ with hole-like excitations. The Fermi level is indicated by dots.

the region $\mathbf{k} \approx N$ (characterized by hole-like excitations) through a gap $\Delta_N/t \approx 0.2$. These topological anomalies are especially significant in the under- and optimal-doped range and for polaron energies above E_p^* . The nodal properties of the new electronic state, stabilized at $E_p = E_p^*$, cannot be classified in terms of Fermi liquid theory.

In our analysis, the nodal non-Fermi liquid (NFL) behavior is also evidenced by an anomalously high scattering rate $\Gamma_{\mathbf{k}_F} = Z_{\mathbf{k}_F} |\text{Im}\Sigma_0^{ph}|$ ($Z_{\mathbf{k}_F}$ is the calculated quasiparticle residue). In Fermi-liquid theory of the free electron gas, one always finds $|\text{Im}\Sigma_0^{ph}| \ll E_2(\mathbf{k})$ sufficiently close to the Fermi level which signifies the existence of coherent quasiparticles with a long life time $\tau = 1/\Gamma_{\mathbf{k}}$. At low T and very close to the Fermi level, the interactions of the free electrons to an Einstein phonon lead to an exponential decrease of $\text{Im}\Sigma_0^{ph} \sim \exp(-\beta\omega_0)$ as $T \rightarrow 0$. This means that

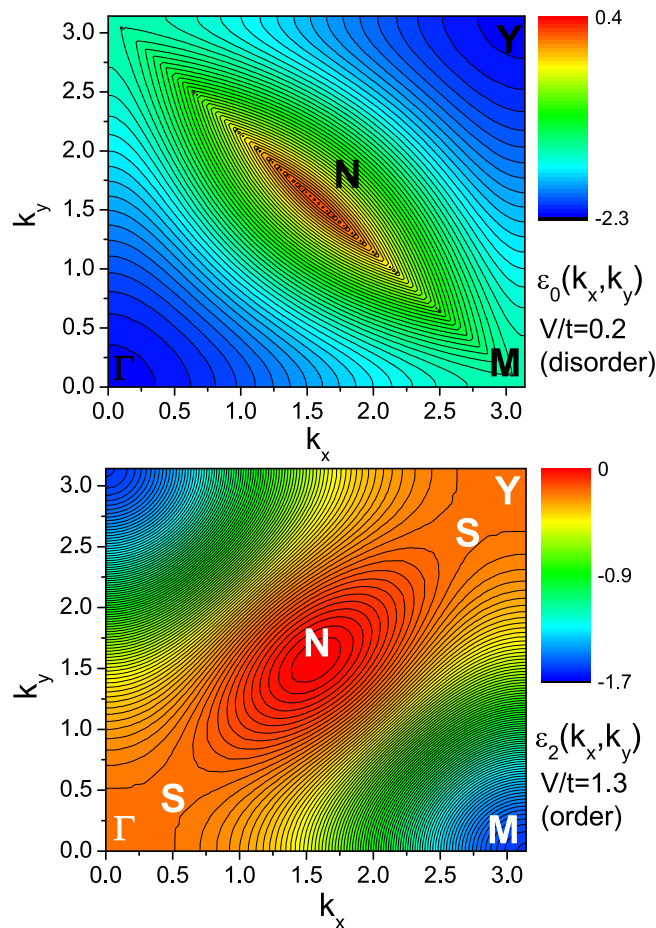


Figure 3. Electronic contour plots of $\varepsilon_0(\mathbf{k}_x, \mathbf{k}_y)$ and $\varepsilon_2(\mathbf{k}_x, \mathbf{k}_y)$ in the disordered ($V/t = 0.2$) and ordered ($V/t = 1.3$) state where the local extremal points are indicated by Γ , M , Y , N , and S . Here $kT/t = 0.03$, $x = 0.11$, $E_p/t = 1.2$.

for small excitation energies ε close to the Fermi level, there always exists a low-temperature range for which $|\text{Im}\Sigma_0^{ph}| \ll \varepsilon$, which is consistent with the concept of Landau quasiparticles [31]. In contrast to this, in the ordered system the nodal electron-phonon scattering near the Fermi level produces a substantial $\text{Im}\Sigma_0^{ph} \sim g^2 \{\log |\Omega_2^S/t| + \log |\Omega_3^S/t| + \eta_N(t, t', V)\} \exp(-\beta\omega_0)$ where the function $\eta_N(t, t', V)$ results from a quadratic expansion of $\varepsilon_2(\mathbf{k})$ in the vicinity of the nodal van-Hove singularities. Due to the large dominant contributions of these van-Hove singularities, in the temperature range $kT/t \leq 0.03$ which is of relevance for the cuprates, we obtain $|\text{Im}\Sigma_0^{ph}| > \varepsilon$ where the excitation energies $\varepsilon \leq kT$ are located close to the Fermi level. The comparison of the corresponding $\text{Im}\Sigma_0^{ph}$ in the free and in the ordered electron gas is presented in Fig. 4. As a consequence, the strong increase of $\text{Im}\Sigma_0^{ph}$ and of the electron scattering rate $\Gamma_{\mathbf{k}_F}$ leads to a violation of the condition for well-defined quasiparticles in the electron-ordered system. We emphasize that the ultimate reason for such a high electron-phonon scattering rate is the anomalously high density of the nodal electronic states related to the flat electron dispersion. The incoherent NFL nodal

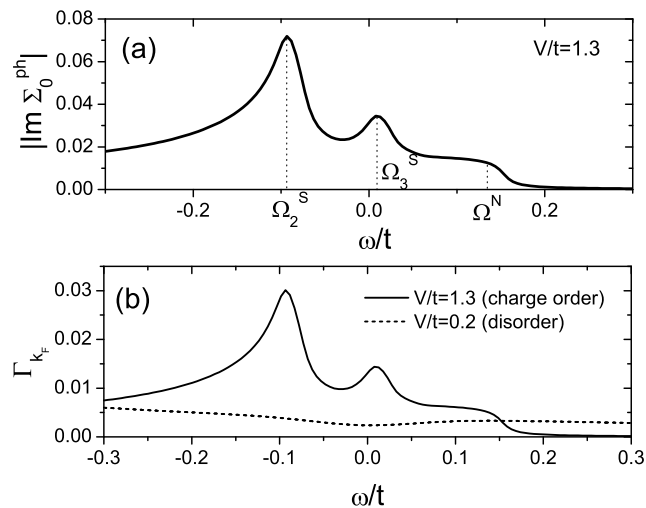


Figure 4. (a) Imaginary part of $\Sigma_0^{ph}(\mathbf{k}, \omega)$ and (b) scattering rate $\Gamma_{\mathbf{k}_F} = Z_{\mathbf{k}_F} |\text{Im} \Sigma_0^{ph}|$ ($Z_{\mathbf{k}_F}$ is the quasiparticle residue) in the charge ordered state (case $V/t = 1.3$, $|\mathbf{k}| = 1.11$) and for the free electron gas ($V/t = 0.2$, $|\mathbf{k}| = 1.3$). Here \mathbf{k} is located in the nodal direction near the N-point of the Brillouin zone, $kT/t = 0.03$, $x = 0.11$, and $E_p/t = 0.2$.

state which develops for $E_p > E_p^*$ is in striking contrast to the Fermi-liquid state with its distinctive hole-type quasiparticle excitations for $E_p < E_p^*$ (dispersion similar to $\varepsilon_2(\mathbf{k})$ in Fig. 2(a)). The existence of the singular multipole structure of the one-electron Green functions and of the anomalously high scattering rates has been confirmed by more elaborate calculations which include higher-order vertex corrections into the electron-phonon contribution to the electronic self-energy. As follows from these calculations, the inclusion of vertex corrections leads to slight shifts of the low-energy van-Hove singularities in $\text{Im} \Sigma_0^{ph}$, without qualitative changes in the nature of the NFL state. In fact, evidence for a NFL behavior along the nodal region, which is even unaffected by the onset of superconductivity, has been found for optimally doped BSCCO [1], in agreement with our findings.

3. Electronic phase separation state

As a state of electronic phase separation would imply a superposition of the ordered and disordered electronic states on the analyzer, the resulting ARPES intensity contains a combination of the disordered ($A^d(\mathbf{k}, \omega)$) and the ordered ($A^o(\mathbf{k}, \omega)$) spectral functions: $I(\mathbf{k}, \omega) = (c_{\text{ord}} A^o(\mathbf{k}, \omega) + c_{\text{dis}} A^d(\mathbf{k}, \omega)) f(\omega)$. Here the coefficients c_{ord} and c_{dis} refer to the ordered and disordered surface fractions. We assume that the ratio $c_{\text{dis}}/c_{\text{ord}}$ depends linearly on doping so that $c_{\text{dis}}/c_{\text{ord}} \sim x$. The consequential dominance of the charge disordered contribution for larger x is consistent with the expansion of metallic disordered regions at higher doping levels as observed in Ref. [16].

Fig. 5 shows the spectral intensity map in the nodal direction calculated for $x =$

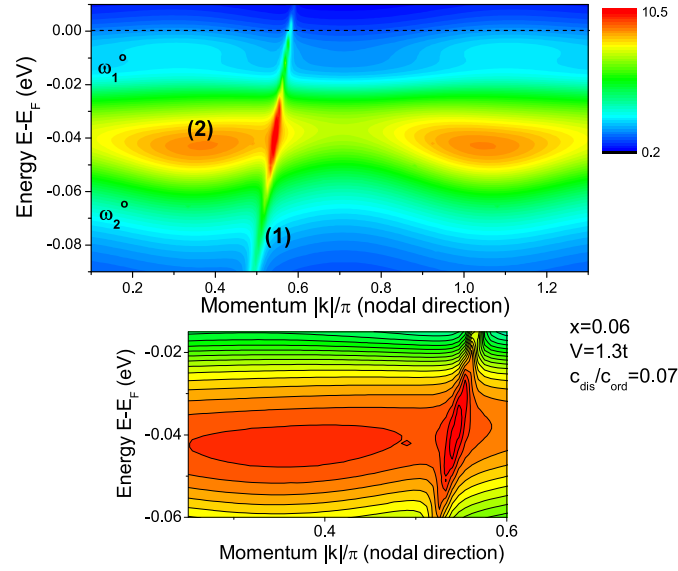


Figure 5. Spectral intensity map $I(\mathbf{k}, \omega)$ for an inhomogeneous electron system with $x = 0.06$ along the nodal direction. The bottom panel displays the detailed structure of the break-up feature at $\omega_2^0 \approx -50$ meV. Here the spectral intensity is renormalized by the weight coefficient of the ordered state c_{ord} ; $V/t = 1.3$, $kT/t = 0.03$, $\omega_0 = 0.05t$ and $E_p = 1.2t$. The position of the Fermi level is indicated by dashed line.

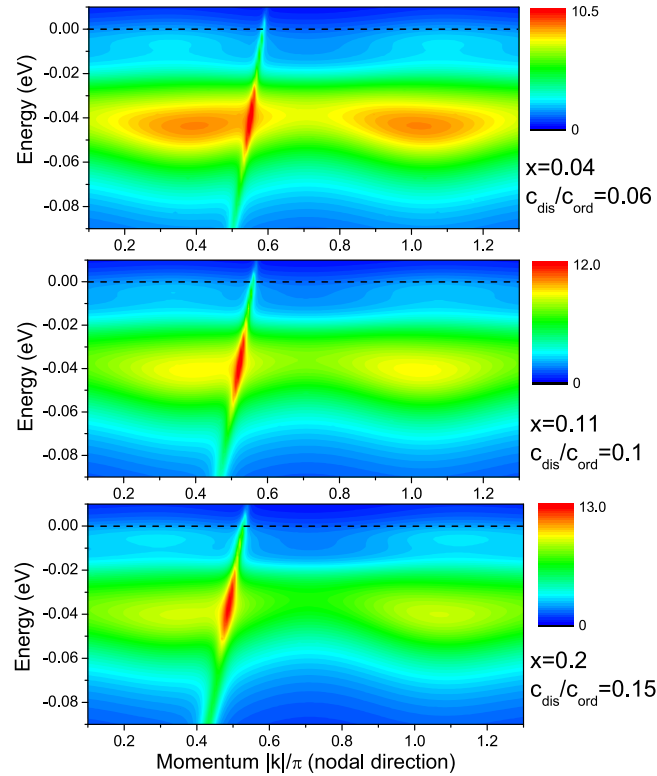


Figure 6. Evolution of the spectral intensity map $I(\mathbf{k}, \omega)$ at different doping levels. The position of the Fermi level is indicated by dashed line.

0.06. One can clearly distinguish two structures on this map. The needle shaped high intensity structure (1) is related to the free electronic band ε_0 . Moreover, a symmetric broad feature (2) appears, originating from the ordered state. The structure (2) is located on the plot in the range between $\omega_2^o \approx -60$ meV and $\omega_1^o \approx -10$ meV. The high spectral intensity of the structure (2) appears due to the singular character of $E_2(\mathbf{k})$ in the vicinity of the point S_1 of the nodal n_1 -region in Fig. 2(c). Near the Fermi level, the NFL-region n_1 forms due to an additional van-Hove singularity at $\omega = \omega_3$ (see Fig. 2(b)) which results in multiple poles of the electronic propagator g_2 and in high spectral intensity in the region between ω_2^o and ω_1^o . In the intensity $I(\mathbf{k}, \omega)$, the ordering-induced feature (2) is superimposed with the free band (1) which produces a break-up of the intensity at $\omega \approx -50$ meV, shown in more detail in the bottom panels of Fig. 5. This break-up of the spectral weight into a quasiparticle peak along the needle (1) and a broad high intensity structure (2) is typical for the nodal ARPES measurements observed in a wide variety of cuprate compounds. As the break-up is produced by the charge-order gap, it should be considered as *a direct manifestation of the local electron order in the cuprates*.

We note that the broad low-energy feature (marked as part (2) in Fig. 5) extends in the \mathbf{k} -direction which is in contrast to the experimental observations. The reason for such a wide spread of this charge-order-induced feature (2) is a simplified approximation for the characteristic phonon frequency $\omega_0 = \text{const}$. Within an Einstein approximation the electron-phonon contribution to the electronic self-energy $\Sigma_{\pm}^{ph}(\omega)$ does not depend on the momentum vector \mathbf{k} , which in turn leads to a wide spread of the self-energy part Σ_2 and of the corresponding high spectral intensity region in the \mathbf{k} -space. To obtain better agreement with experiment, where the high-intensity structure is localized in \mathbf{k} -space, one needs to consider a realistic description for the phonon dispersion which is beyond the scope of our current studies.

Due to the doping dependence of $\Sigma_2(\mathbf{k}, \omega)$, the high intensity features also depend strongly on doping which is demonstrated in Fig. 6. The high-intensity structure, at about -50 meV for $x = 0.04$, becomes smoother with increasing x up to $x = 0.11$ and in the overdoped regime ($x = 0.2$ in Fig. 6). Moreover, as the local order is destroyed with increasing T , the contribution of ordered domains to $I(\mathbf{k}, \omega)$ will decrease which can explain the fact of vanishing kinks for higher T discussed in Refs. [5] and [32].

The interpretation of ARPES intensities in terms of electronic inhomogeneities is a possible scenario not only for cuprates, but can be applied also for manganite compounds. In manganites, a significant electron-phonon coupling and an electronic phase separation of ferromagnetic metallic and charge ordered states is strongly supported by numerous experimental and theoretical studies [33, 34, 35]. Consequently, the nodal ARPES features reported for $\text{La}_{1.2}\text{Sr}_{1.8}\text{Mn}_2\text{O}_7$ [36] can also be explained by the proposed approach for inhomogeneous states.

In conclusion, we show that coupling to phonon modes leads to different spectral properties in ordered and disordered electronic states. It appears to be the key mechanism responsible for the main features detected in ARPES experiments of high- T_c

cuprates. The broad character of the ARPES features can be related to the incoherent nature of the nodal non-Fermi-liquid state which forms essentially due to the electron-phonon coupling. In this context, the implications of electron-phonon coupling in charge ordered systems demonstrate in a novel way how collective modes can qualitatively change the fundamental properties of the electron liquid.

This work was supported by Deutsche Forschungsgemeinschaft through SFB 484.

References

- [1] Valla T *et al.* 1999 *Science* **285** 2110
- [2] Lanzara A *et al.* 2001 *Nature* **412** 510
- [3] Zhou X J *et al.* 2005 *Phys. Rev. Lett.* **95** 117001
- [4] Borisenko S V *et al.* 2006 *Phys. Rev. Lett.* **96** 117004
- [5] Kordyuk A A *et al.* 2006 *Phys. Rev. Lett.* **97** 117002
- [6] Damascelli A, Hussain Z, and Shen Z H 2003 *Rev. Mod. Phys.* **75** 473
- [7] Yunoki S, Dagotto E, and Sorella S 2005 *Phys. Rev. Lett.* **94** 037001; Mishchenko A S and Nagaosa N 2004 *Phys. Rev. Lett.* **93** 036402
- [8] Hengsberger M *et al.* 1999 *Phys. Rev. Lett.* **83** 592
- [9] Valla T, Fedorov A V, Johnson P D, and Hulbert S L 1999 *Phys. Rev. Lett.* **83** 2085
- [10] Byczuk K *et al.* 2006 *Nature Physics* **3** 168
- [11] Pavlenko N and Kopp T 2006 *Phys. Rev. Lett.* **97** 187001
- [12] Brown S E, Fradkin E, and Kivelson S A 2005 *Phys. Rev. B* **71** 224512
- [13] Howald C *et al.* 2003 *Phys. Rev. B* **67** 014533
- [14] Kivelson S A *et al.* 2003 *Rev. Mod. Phys.* **75** 1201
- [15] Vershinin V *et al.* 2004 *Science* **303** 1995
- [16] Kohsaka Y *et al.* 2004 *Phys. Rev. Lett.* **93** 097004
- [17] Giustino L, Cohen M L, and Louie S G 2008 *Nature* **24** 975
- [18] Heid R, Bohnen K P, Zeyher R, and Manske D 2008 *Phys. Rev. Lett.* **100** 137001
- [19] Cuk T *et al.* 2005 *phys. stat. sol. (b)* **242** 11
- [20] Kohsaka Y *et al.* 2007 *Science* **315** 1380
- [21] Tranquada J M *et al.* 1995 *Nature* **375** 561
- [22] Hoffman J E *et al.* 2002 *Science* **295** 466
- [23] Hanaguri T *et al.* 2004 *Nature* **430** 1001
- [24] Lee J *et al.* 2006 *Nature* **442** 546
- [25] Pan S H *et al.* 2001 *Nature* **413** 282
- [26] Singer P M, Hunt AW, and Imai T 2002 *Phys. Rev. Lett.* **88** 047602
- [27] Ofer R, Levy S, Kanigel A, and Keren A 2006 *Phys. Rev. B* **73** 012503
- [28] Abbamonte P *et al.* 2005 *Nature Physics* **1** 155
- [29] Eschrig M and Norman M R 2003 *Phys. Rev. B* **67** 144503
- [30] Platé M *et al.* 2005 *Phys. Rev. Lett.* **95** 077001
- [31] Abrikosov A A, Gorkov L P, and Dzyaloshinski I E 1975 *Methods of quantum field theory in statistical physics* (New York: Dover)
- [32] Johnson P D *et al.* 2001 *Phys. Rev. Lett.* **87** 177007
- [33] Roder H, Zhang J, and Bishop A R 1996 *Phys. Rev. Lett.* **76** 1356
- [34] Moreo A, Yunoki S, and Dagotto E 1999 *Science* **283** 2034
- [35] Dagotto E, Burgy J, and Moreo A 2003 *Solid State Communications* **126** 9
- [36] Mannella N *et al.* 2005 *Nature* **438** 474